Manuscript ID: 1370
DOI: 10.18462/iir.icr.2019. 1370

Thermodynamic analysis of an absorption heat transformer based on experimental measurements

José L. CORRALES CIGANDA [(a)], Falk CUDOK [(a)], Manuel WAHL [(a)], Marvin SCHLOESSER [(a)], Dominik METZNER [(a)]

[(a)] Institut für Energietechnik, Technische Universität Berlin
Marchstr. 18, Berlin, 10587, Germany, jose.l.corralesciganda@tu-berlin.de

ABSTRACT

A prototype of an absorption heat transformer with a nominal capacity of 40 kW recovered heat has been investigated and compared with another prototype which measurements have been presented in a previous work (Cudok et al., 2017). The new prototype has been designed for upgrading industrial waste heat by recovering it at a temperature between 80 and 100°C and boosting it to a temperature level between 120 and 150°C. External heat balances obtained from measured external temperatures and flow rates combined with internal balances from enthalpy calculations of liquid and vapor flows have been used to get more insight into the internal process as occuring in real operation. The amount of adiabatic absorption in the absorber has been assessed (amounts up to 30% of the total referigerant absorbed), explaining the resulting heat flows int the main heat exchangers.
Moreover, an observed malfunction consisting of liquid refrigerant carry over from evaporator to absorber could be quantified with the results of the energy balances, explaining the deviation between measured coefficients of performance and expected ones.
Keywords: Heat Recovery, Enthalpy, Energy Balance, Absorption, Laboratory.

1. INTRODUCTION

This work aims to analyze the internal process of an absorption heat transformer (AHT) based on laboratory measurements, and to understand the differences between expected and obtained values for the coefficient of performance (COP). Two AHT prototypes are analysed by means of mass and energy balances: the first one presented in previous work, is able to work as an absorption chiller / heat pump or as a heat transformer (pr I). The second one (pr II) is based on the first one, but is adapted to be used only as a heat transformer and includes additional temperature sensors.

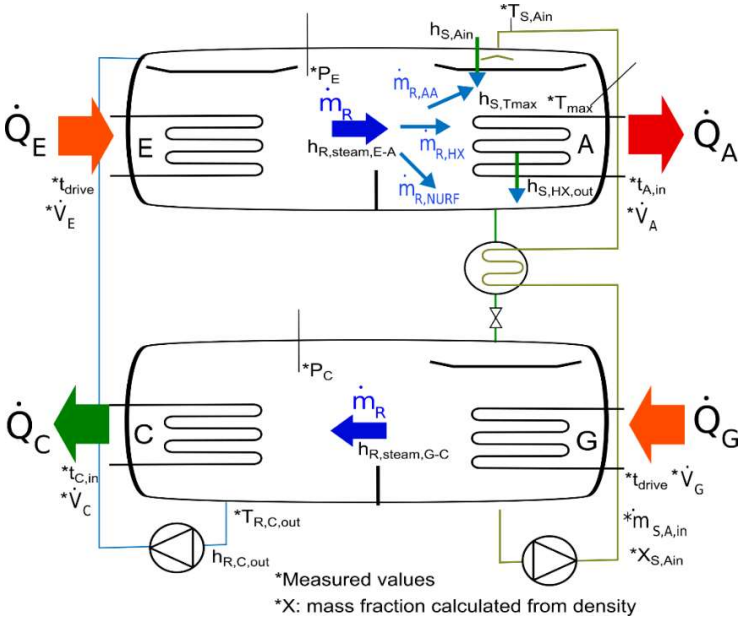

Figure 1: Absorption heat transformer scheme with measured values

, Measurement results of pr I have been presented in a previous work (Cudok et al., 2017) including the externally measured heat flows and a first estimation of the heat transfer coefficients. The same testrig used for pr I is used for the tests of pr II, that has been built with slighty different heat exchanger areas as table 1 shows. In a previous work, simulations of the AHT using different tools and thermodynamical property models but same physical model have been compared with one of the earliest measurements of the first prototype (Corrales Ciganda et al., 2016). This model has been used to define the new areas.

Prototype	A_A (m^2)	A_G/A_A (-)	A_E/A_A (-)	A_C/A_A (-)	$\dot{V}_{X=A,G,C,E}$ (m^3/h)	$\dot{m}_{sol}$ (kg/h)	$t_{C,in}$ (°C)	$t_{drive}=t_{GE,in}$ (°C)	$t_{A,in}$ (°C)
pr I	7.6	1	1	1	5	700	25-40	60-95	80-130
pr II	8.2	1.1	0.8	0.7	5	700	25/35	85/90/95	130

Table 1. HX Areas and measurement conditions for prototypes pr I and pr II

In this work, the results obtained with pr II are compared with the results obtained with pr I. Heat balances using external heat flows and internal mass and enthalpy flows have been calculated to understand the differences in the obtained results, and are used to derive the effectiveness of certain internal processes. These analyses revealed some inefficiencies that are usually not taken into account in most thermodynamical models of the cycle, and explain the differences between expected and measured COPs.

2. MEASUREMENTS: EXTERNAL HEAT FLOWS ANALYSIS

2.1. Experimental Results: Revaluated Heat Flows and COP

Fig. 2 presents the recovered heat flow rates measured for each AHT prototype ($\dot{Q}_A$) and its coefficient of performance, as a function of the double temperature difference $\Delta\Delta t$. The double temperature is an indicator for the driving temperature of the AHT, as presented in (Cudok & Ziegler, 2015) calculated using the definition from Eq. (1):

$$\Delta\Delta t = (t_G - t_A) - B \cdot (t_C - t_E) = B \cdot (t_E - t_C) - (t_A - t_{GE}) \qquad \textit{Eq. (1)}$$

The coefficient of performance for an AHT is defined as the useful high temperature heat flow rate transferred in the absorber divided by the total amount of waste heat flow rate transferred in generator and evaporator:

$$COP = \frac{\dot{Q}_A}{Q_G + \dot{Q}_E} \qquad \textit{Eq. (2)}$$

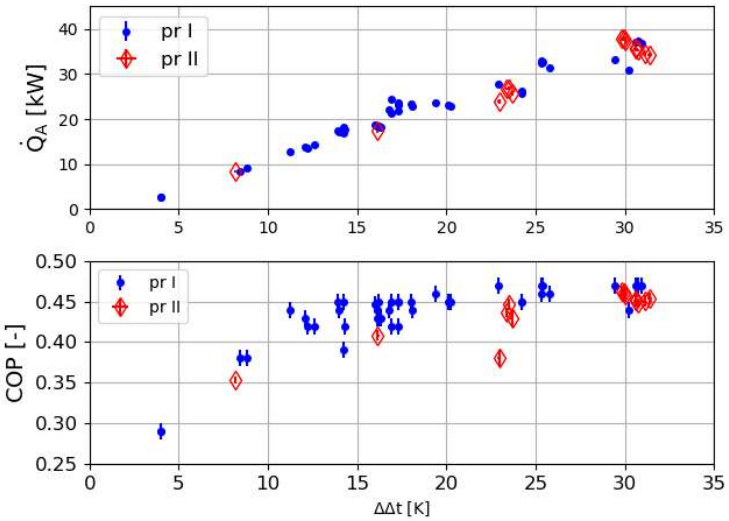

Figure 2: $\dot{Q}_A$ and COP vs. $\Delta\Delta t$ for pr I and pr II

Three sets of operating conditions have been consistently measured for pr II. The conditions correspond to the expected ones for a pilot plant prototype to be installed in the last phase of the Indus3Es project. The temperatures of the waste heat source have been variated between 85, 90 and 95°C with fixed inlet temperatures for the cooling water ($t_{C,in}$ =25°C) and for the higher temperature useful heat stream ($t_{A,in}$=130°C).These points had been previously measured for pr I and will be the basis for following analysis. For all measuremensts, flow rates at external circuits and solution pump has been set constant as presented in Table I.

The recovered higher temperatures heat flow rates measured with pr II are very similar to those measured with pr I. For example, for waste heat source temperatures of 95°C (ΔΔt around 30 K) the heat flow rates for pr I are between 36.9 and 37.4 kW. For the same waste heat source temperatures the results of pr II are between 34.3 and 37.8 kW, with a much bigger scatter. Regarding the COP, the values obtained for pr II are lower for the same operation conditions than those obtained for pr I.The differences seems to become bigger for points with lower ΔΔt values and lower heat flows. The differences could be caused by:

- Presence of non condensables gases during pr II measurements.
- Differences in effectiveness of the solution heat exchanger (SHX)
- Differences in heat losses to the surrounding environment
- Differences in adiabatic absorption efficiencies for same operation conditions
- Differences in non-usable refrigerant flows (NURF) between evaporator and absorber

The pressence of non-condensable gases has been investigated but could not be detected for any measurement. The effectiveness of the solution heat exchanger was calculated with measured temperatures and resulted in values between 77 and 81% for all tests of both prototypes (no significant differences). The following sections investigate if either differences in heat losses, differences in adiabatic absorption rates or differences in the amount of non-usable refrigerant flows can give a hint for the differences observed in the measurements.

2.2. AHT Energy Balances and Possible Heat Losses

If the heat balance of the AHT differs from zero at least one of the assumptions made for modelling is not valid. Either is the AHT not adiabatic or the measurements are not completely under steady state (thermal masses inside the AHT being still heated up or cooled down). Using all four heat flows entering/leaving the AHT we can write:

$$\dot{Q}_{bal,AHT} = \dot{Q}_A + \dot{Q}_G + \dot{Q}_E + \dot{Q}_C \qquad \textit{Eq. (3)}$$

Being $\dot{Q}_X$ the measured heat flow rates, that are positive when entering the AHT and negative when leaving it. Thus, a positive value for $\dot{Q}_{bal,AHT}$ indicates that heat is being stored within the AHT system or transferred to the surrounding environment (heat losses).

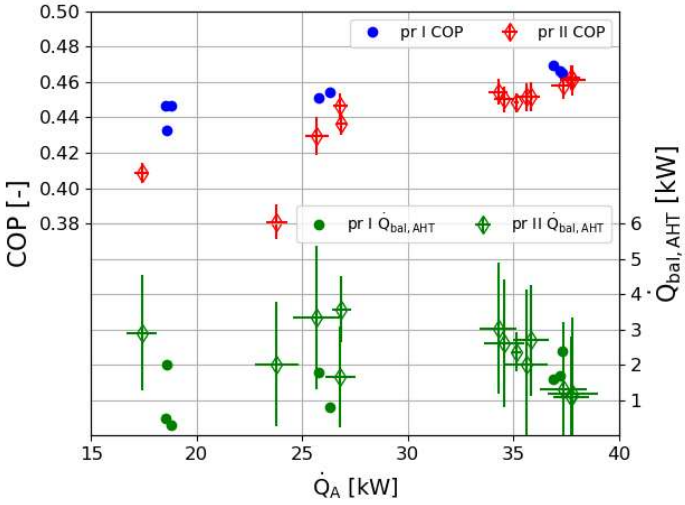

Figure 3: COP and $\dot{Q}_{bal,AHT}$ vs $\dot{Q}_A$ for pr I and pr II

Positive values for $\dot{Q}_{bal,AHT}$ are obtained for all measurements. Taking into consideration the measurement uncertainty, it can be affirmed for all measurements that the value for the unbalanced

heat flow lays between 0 and 5 kW. For measurements with $\dot{Q}_{,A}$ between 34 and 40 kW (t_{drive}=95°C) the obtained COP values for pr II (0.45-0.47) are similar to those of pr I (0.47) Same can be observed for measurements with revaluated heat flow around 25kW (t_{drive}=90°C) For even smaller $\dot{Q}_{,A}$ values (t_{drive}=85°C) the differences in obtained COP between pr I (0.41) and pr II (0.43-0.45) are beyond the measurement uncertainty. For this measurement with lower heat flow rates the influences of the non balanced heat flows on the COP is bigger. With an ideal zero value heat balance for the AHT, the difference between pr I and pr II COP values would be reduced : if the non balanced heat flows are substracted from the useful heat, the COP values would lay between 0.45 and 0.48 for pr I and between 0.43 and 0.47 for pr II. Other irreversibilites different than the heat losses must be responsible of the remaining difference.

3. MEASUREMENTS: INTERNAL ENTHALPY FLOWS ANALYSIS

3.1. Adiabatic Absorption

Another possible reason for the differences found between measured recovered heat flow rates for pr I and pr II is that the efficiency of the adiabatic absorption process is different.
In Fig. 1 the streams involved in the adiabatic absorption process are presented. The amount of refrigerant ideally adiabatically absorbed is calculated assuming adiabatic mixing and absorption up to saturated state. This can be expressed with the following equations, which are solved simultaneously using thermodynamic property functions and measured data: vessel pressure, and measured temperature, mass fraction and mass flow rate of the solution entering the absorber.

$$\dot{m}_{S,A,in} + \dot{m}_{R,AA,ideal} = \dot{m}_{S,Tmax,ideal} \qquad \textit{Eq. (4)}$$

$$\dot{m}_{S,A,in} \cdot h_{S,A,in} + \dot{m}_{R,AA,ideal} \cdot h_{R,steam,E-A} = \dot{m}_{S,Tmax,ideal} \cdot h_{S,Tmax,ideal} \qquad \textit{Eq. (5)}$$

$$\dot{m}_{S,A,in} \cdot X_{S,A,in} = \dot{m}_{S,Tmax,ideal} \cdot X_{S,Tmax,ideal} \qquad \textit{Eq. (6)}$$

with
$h_{\mathrm{S,A,in}} = h(p_{\mathrm{E}}, T_{\mathrm{S,A,in}}, X_{\mathrm{S,A,in}})$,$h_{\mathrm{S,Tmax,ideal}} = h_{\mathrm{sat}}(p_{\mathrm{E}}, X_{\mathrm{S,Tmax,ideal}})$, $T_{\mathrm{max,ideal}} = T_{sat}(p_{\mathrm{E}}, X_{\mathrm{S,Tmax,ideal}})$

once $T_{\mathrm{max,ideal}}$ is obtained, the adiabatic absorption effectiveness can be defined as:

$$\eta_{AA} = \frac{T_{max,meas} - T_{S,A,in}}{T_{max,ideal} - T_{S,A,in}} \qquad \textit{Eq. (7)}$$

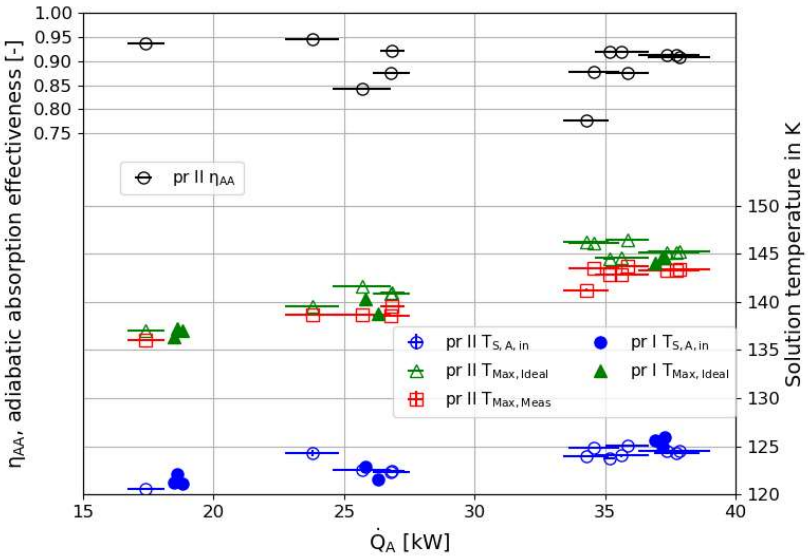

Figure 4: η_{AA} for pr II and measured temperatures for pr I and pr II

By comparing the maximal temperature measured after adiabatic absorption at the vessel with the ideal maximal temperature from the calculations above, we can obtain a value for the effectiveness of the adiabatic absorption.
The effectiveness calculations are presented only for measurements with pr II because measurements of the solution temperature inside the absorber after adiabatic absorption were not included when pr ! was investigated. Since the maximum temperature inside the vessel could be higher than the maximum temperature measured at the surface of the first tube rows of the absorber, the adiabatic absorption effectiveness could be higher than the presented values. Nevertheless, the values obtained are quite high (between 85 and 95%) and similar for all measured points. The differences between adiabatic absorption effectiveness calculated for prI and por II are not significant and do not seem to be the reason for neither the differences in COPs nor for the scatter in revaluated heat flow rates. Pr II was designed in order to obtain better adiabatic absorption than for pr I, so the adiabatic absorption effectiveness for pr I is expected to be lower.

3.2. Non-Usable Refrigerant Flows (NURF)

The non-usable refrigerant flows (NURF) can be defined as refrigerant flows between evaporator and absorber other than those being absorbed adiabatically or at the surface of the absorber heat exchanger tube bundles.
The total amount of refrigerant flow rate between generator and condenser is obtained from an energy balance at the condenser with the assumption of an condensation process without heat losses in steady state. The measured temperature of the liquid refrigerant leaving the condenser and the measured pressure inside the lower pressure vessel are used for the calculations.

$$\dot{m}_R = \frac{\dot{Q}_C}{(h_{R,steam,C-E} - h_{R,C,out})} \qquad \textit{Eq. (8)}$$

with

$$h_{R,steam,C-E} = h_{steam}(p_C, t_{drive}) \qquad \textit{and} \qquad h_{R,C,out} = h_{liquid}(p_C, T_{R,C,out})$$

In steady state conditions, the refrigerant mass flow rate from evaporator to absorber is the same as the flow rate from generator to condenser. At the same time, for an ideally insulated absorber this flow rate should be equal to the addition of the refrigerant flows adiabatically absorbed ($m_{R,AA}$) and absorbed at the tube bundle surface ($m_{R,HX}$). Writing an energy balance around the absorber we get

$$\dot{m}_{S,A,in} + (\dot{m}_{R,AA,ideal} + \dot{m}_{R,HX,ideal}) = \dot{m}_{S,HX,out} \qquad \textit{Eq. (9)}$$

$$\dot{m}_{S,A,in} \cdot h_{S,A,in} + (\dot{m}_{R,AA,ideal} + \dot{m}_{R,HX,ideal}) \cdot h_{R,steam,E-A} = m_{S,HX,out} \cdot h_{S,HX,out} \qquad \textit{Eq. (10)}$$

$$\dot{m}_{S,A,in} \cdot X_{S,A,in} = \dot{m}_{S,HX,out} \cdot X_{S,HX,out} \qquad \textit{Eq. (11)}$$

with $h_{R,steam,E-A} = h_{steam,sat}(p_E)$ *and* $h_{S,HX,out} = h_{sat}(p_E, X_{S,HX,out})$.

According to the definition for NURF given above, we can write:

$$\dot{m}_{NURF} = \dot{m}_R - \left(\dot{m}_{R,AA,ideal} + \dot{m}_{R,HX,ideal}\right) = \dot{m}_R - (\dot{m}_{R,AA} + \dot{m}_{R,HX}) \qquad \textit{Eq. (12)}$$

The obtained mass flow rates are plotted together with $\dot{m}_{R,AA}$ obtained with equations (4) to (6).
From the values obtained and shown in Fig. 5 it can be concluded that for the same revaluated heat output prototype pr I operates with less refrigerant flow rate than pr II.
The flow of adiabatically absorbed refrigerant is really similar for measurements with pr I and pr II, and accounts for around 18-20% of the total refrigerant flow in measurements with capacities between 35-40 kW and up to 29% for capacities around 18 kW. The calculated (minimal) amounts of NURF for measurements of pr II are between 2 and 5 times those (minimal) amounts calculated for measurements of pr I. These conclusions, however, must be taken very carefully, since the values obtained for NURF are within the uncertainty range for the calculated refrigerant mass flow rates.

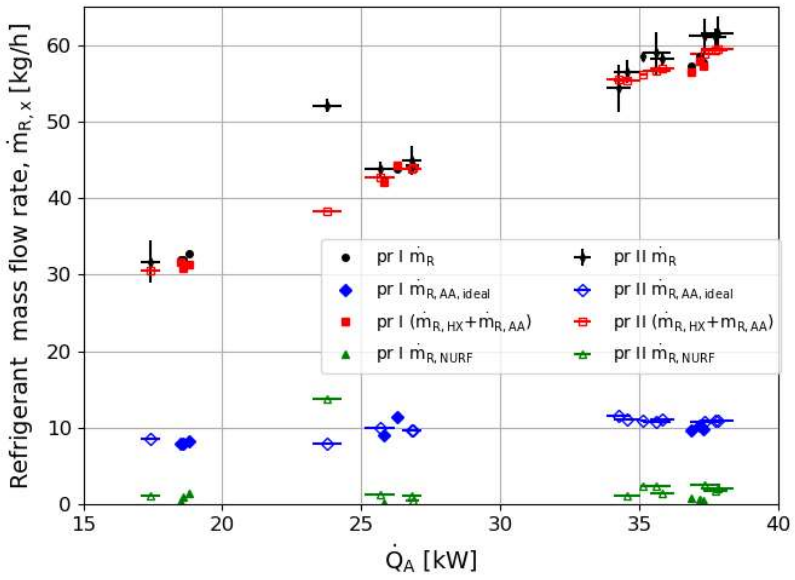

Figure 5: Refrigerant mass flow rates vs $\dot{Q}_A$

As explained in the text above, there is a mass flow of the non usable refrigerant flows from the evaporator into the absorber sump bypassing the heat exchanger tubes. It is possible that liquid refrigerant sprinkles directly into the absorber sump. It is also possible that refrigerant vapor flows from the evaporator to the absorber chamber, condenses at the shell tube and flows afterwards into the sump. A mixture of both procedures is also possible. In the case of liquid droplets the condenser and generator have to condense respectively generate that amount of non usable refrigerant on top of the refrigerant absorbed at the absorber. The evaporator evaporates the same amount of refrigerant the absorber absorbs. In the case of condensation at the shell tube at the absorber, the evaporator needs to evaporate the refrigerant absorbed by the absorber and additional the refrigerant condensed at the shell tube. In case liquid droplets the influence to the COP will be lower than in case refrigerant vapor condense at absorber shell tube.
To understand the influence of this non usable mass flow to the COP, its value excluding the heat input related to non-usable refrigerant flow for its calculation will be estimated. For the case “liquid refrigerant droplets” the following equations are used:

$$COP_{ld} = \frac{\dot{Q}_A}{(\dot{Q}_G - \dot{Q}_{G,NURF}) + \dot{Q}_E} \qquad \textit{Eq. (13)}$$

The heat flow for the additional vapor generation in the generator is estimated by multiplication of the non-usable refrigerant mass flow rate and the specific heat of dilution $(r + l)$:

$$\dot{Q}_{G,NURF} = \dot{m}_{R,NURF} \cdot (r + l) \qquad \textit{Eq. (14)}$$

In case of “vapor condensation” at the tube shell the corrected COP depends on the on $\dot{Q}_{G,NURF}$ and $\dot{Q}_{E,NURF}$ as following:

$$COP_{vd} = \frac{\dot{Q}_A}{(\dot{Q}_G - \dot{Q}_{G,NURF}) + (\dot{Q}_E - \dot{Q}_{E,NURF})} \qquad \textit{Eq. (15)}$$

With

$$\dot{Q}_{E,NURF} = \dot{m}_{R,NURF} \cdot r \qquad \textit{Eq. (16)}$$

The relation between the heat of vaporization r and the heat of dilution $(r + l)$ is described by the Dühring factor B (Ziegler, 1997):

$$r \cdot B = (r + l) \qquad \textit{Eq. (17)}$$

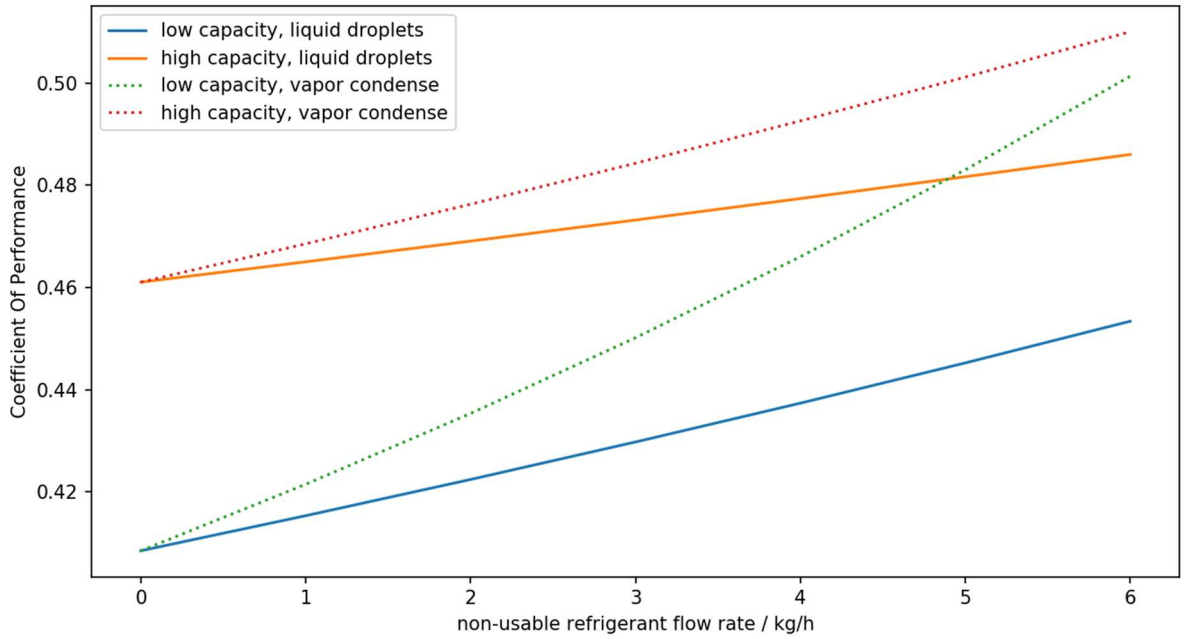

Figure 6: Effect of NURF on the COP

For two measurements, one with with low capacities ($\dot{Q}_{\mathrm{A}} = 17.39\ \mathrm{kW}, \dot{Q}_{\mathrm{E}} = 23.23\ \mathrm{kW}, \dot{Q}_{\mathrm{G}} = 19.34\ \mathrm{kW}$) and one with high capacities ($\dot{Q}_{\mathrm{A}} = 37.83\ \mathrm{kW}, \dot{Q}_{\mathrm{E}} = 43.10\ \mathrm{kW}, \dot{Q}_{\mathrm{G}} = 38.95\ \mathrm{kW}$) a variation of the non usable refrigerant mass flow rate ($0 \geq \dot{m}_{\mathrm{R,NURF}} \geq 6\ \mathrm{kg \cdot m^{-2}}$) by adaption the Eqs. (13) to (17) was done (see Fig. 6) In addition, it was assumed $r = 2200\ kJ/kg$ and $B = 1.15$.
This figure shows the corrected COP depending on the assumed non usable refrigerant flow. The mean value of the non usable refrigerant flow is around 4kg/h for the presented measurements (see Fig. 5). For the low capacity the corrected COP would be 44%, when the case “liquid droplets” will be compensated, and 46%, when the case “vapor condensate” will be compensate, instead of the measured COP of 41%. For the high capacity the measured COP of 46% will be corrected to 48% or 49% respectively. The diagram shows both case separately. The results of a non usable mass flow consist of sprinkling liquid droplets and condensing vapor will be between the particular curves.

4. CONCLUSIONS

The $\dot{Q}_{,\mathrm{A}}$ values measured with pr II are in the same range and only slightly smaller than those obtained for pr I and presented in (Cudok et al., 2017). The obtained COPs with pr II measurements were in in almost all cases lower than those obtained with measurements of pr I. One of the reasons for these differences in COP is the difference in heat losses to the surroundings, that was between 1 and 1.5 kW higher for pr II than for pr I, according to the energy balances.
The flow of refrigerant being adiabatically absorbed accounts for up to 30% of the total refrigerant flow. Calculated using the maximum temperature measurements inside the absorber of prototype pr II, at least 17% to 25% of the total flow of refrigerant is absorbed adiabatically (adiabatic absorption efficiencies in the range of 85-95%). It does not seem likely that differences in adiabatic absorption explain the differences in COP between pr I and pr II.
Higher Non Usable Refrigerant Flows (NURF) values have been obtained for pr II than for pr I. This NURF can be either liquid drops flow from the evaporator distribution system into the absorber sump, or steam flow condensing at any vessel surface. The amount of NURF is estimated to be between 2 and 7% of the refrigerant flow. This can reduce the COP between 1 and 3 percentual points.
Based on these analyses, differences in COP between the two prototypes can be explained by of the higher NURF values and increased heat losses for pr II compared to pr I. However, the scatter in recovered heat flows (up to 8%) for measurements of pr II under the same conditions cannot be explained by these reasons. The main hypothesis for this scatter in recovered heat flows is the different wetting of the absorber heat exchanger tube bundles during some tests, due to corrosion and particle accumulation in the solution circuit.

ACKNOWLEDGEMENTS

This work has been developed under the project “Indus3Es: Industrial Energy and Environmental Efficiency” funded by the Horizon 2020 framework of the European Union, Project No. 680738. http://www.indus3es.eu

NOMENCLATURE

Symbols

A	Heat exchanger area (m²)	p	pressure (kPa)
AHT	Absorption heat transformer	pr I / II	Prototype 1 / 2
B	Dühring factor	$\dot{Q}$	Heat flow (kW)
COP	Coefficient of performance	r	Spec. heat of vaporization (kJ×kg^{-1})
DDT	Double temperature difference (K)	$r+l$	Spec. heat of dilution (kJ×kg^{-1})
η	Effectiveness	SHX	Solution heat exchanger
h	Spec. enthalpy (kJ×kg^{-1}×K^{-1})	t	External temperature (°C)
$\dot{m}$	Mass flow (kg×s^{-1})	T	internal temperature (°C)
NURF	Non-usable refrigerant flow	X	Mass fraction (kg×kg^{-1})

Indices

A	Absorber	max	Maximal
AA	Adiabatic absorption	meas	Measurements
Bal	Energy balance	NURF	Non-usable refrigerant flow
C	Condenser	out	Outlet
drive	Driving	R	Refrigerant
E	Evaporator	rec	Recirculation at E
G	Generator	revaluated	Revaluated
HX	Heat exchanger bundle	S	Solution
in	Inlet	sat	Saturated
ld	Liquid droplets	*steam*	Steam
liquid	Liquid	*th*	Thermal
Ideal	Ideal		

REFERENCES

Corrales Ciganda, J. L. et al., 2016. Thermodynamic cycle models for the development of absorption heat transformers for the process industry. Nottingham, s.n., p. paper 320.

Cudok, F., Corrales Ciganda, J. L. & Kononenko, N., 2017. Experimental Results of an absorption heat transformer. Rotterdam, s.n., p. O 4.4.2.

Cudok, F. & Ziegler, F., 2015. Absorption heat converter and the characteristic equation method. Yokohama, s.n., p. paper 764.

Ziegler, F., 1997. Sorptionswärmepumpen. Erding: Forschungsberichte des Deutschen Klima- und Kältetechnischen Vereins e.V..